ISBN: 978-3-95450-208-0 doi:10.18429/JACoW-IPAC2019-MOPGW060

CHERENKOV RADIATION AT OFF-AXIS BUNCH PASSAGE THROUGH DIELECTRIC CONCENTRATOR*

S. N. Galyamin†, A. V. Tyukhtin, V. V. Vorobev
St. Petersburg State University, 7/9 Universitetskays nab., St. Petersburg, 199034 Russia

Abstract

Here we procceed with investigation of all-dielectric target which concentrate Cherenkov radiation (CR) near the predetermined focus and increase the field up to several orders of magnitude, so called "concentrator for CR". We consider a non-symmetrical case where charge trajectory has a shift with respect to structure axis. We develop analytical approach for CR investigation and present typical numerical results.

INTRODUCTION

Today several modern trends based on beam-dielectric interaction exist in accelerator physics. One should mention dielectric wakefield acceleration technique which is now operating with Terahertz (THz) wakefields [1] and has demonstrated Gigavolt per meter fields [2]. With this scheme, dielectric-lined waveguides, i.e. "closed" structures with dielectric, are utilized. Similar structures are also considered as prospective candidates for contemporary beam-driven sources of THz radiation [3]. On the other hand, various "open" dielectric structures are extensively studied nowadays in view of development of both beam-driven radiation sources [4] and non-invasive bunch diagnostics systems [5,6] It is worth noting that rigorous theoretical explanation of Cherenkov radiation (CR) emerging during the interaction of charged particle with dielectric object of finite size is extremely complicated, therefore various approximate methods are used. We utilize and develop our own combined approach recently approved by numerical simulations in COMSOL Multiphysics [7] and possessing the asymptotic accuracy [8,9]. This approach has been utilized to determine the outer profile of "concentrator for CR": axisymmetric dielectric target concentrating the majority of generated CR in a small vicinity of a predetermined focus without any additional lenses or mirrors [10]. This target was investigated in details for symmetric case [7, 11]. For practice, it also important to analyze the influence of trajectory offset from the symmetry axis to the radiation characteristics. This is the main goal of this report.

CONCENTRATOR GEOMETRY

Figure 1 shows geometry of the problem: a point charge q moves with constant velocity $v = \beta c$ along straight trajectory inside the channel in axisymmetric dielectric target with permittivity ε and permeability $\mu = 1$. Position of charge's trajectory is determined by r_0 and φ_0, see Fig. 1 (b).

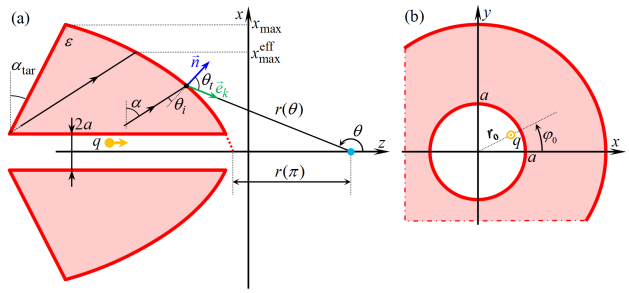

Figure 1: Geometry of the problem. (a) (zx)-cut of dielectric concentrator for CR. (b) (xy)-cut of the target and position of the charge's shifted trajectory.

Cylindrical coordinates $\rho = \rho_0, z = z_0$ of the outer profile of the target have been determined for $r_0 = 0$ earlier [10]:

$$\rho_0(\theta) = r(\theta)\sin(\theta), \quad z_0(\theta) = z_f + r(\theta)\cos(\theta),$$
$$r(\theta) = f(1-\sqrt{\varepsilon})\left[1+\sqrt{\varepsilon}\sin(\alpha+\theta)\right]^{-1}, \tag{1}$$

where $\alpha = \arcsin[1/(\sqrt{\varepsilon}\beta)]$ and f is a "focal" parameter. Maximum transverse size of the target x_{max} determines minimum angle θ_{min}, maximum angle θ_{max} is determined by the channel radius a.

STRATTON-CHU FORMALISM

According to our combined approach, we utilize the Stratton-Chu formulas [12] to calculate CR exiting the target using tangential components of EM field at the aperture S_a:

$$4\pi\vec{E}_\omega = \int_{S_a}\left\{ik_0\left[\vec{n},\vec{H}^a_\omega\right]\psi + \right.$$
$$\left. + \frac{i}{k_0}\left(\left[\vec{n},\vec{H}^a_\omega\right],\vec{\nabla}\right)\vec{\nabla}\psi + \left[\left[\vec{E}^a_\omega,\vec{n}\right],\vec{\nabla}\psi\right]\right\}d\Sigma, \tag{2}$$

where $k_0 = \omega/c$, $d\Sigma = \sqrt{g}d\theta d\varphi$,

$$\sqrt{g} = \frac{-f^2(1-\sqrt{\varepsilon})^2\sin\theta\sqrt{1+\sqrt{\varepsilon}\sin(\theta+\alpha)+\varepsilon}}{\left[1+\sqrt{\varepsilon}\sin(\theta+\alpha)\right]^3},$$

$\psi = \exp\left(ik_0\tilde{R}\right)/\tilde{R}$, $\tilde{R} = \sqrt{(x-x_0)^2+(y-y_0)^2+(z-z_0)^2}$, $\vec{n}$ is a unit normal,

$$\begin{Bmatrix} n_\rho \\ n_z \end{Bmatrix} = \left[\begin{Bmatrix} \sin\theta \\ \cos\theta \end{Bmatrix} + \sqrt{\varepsilon}\begin{Bmatrix} \cos\alpha \\ \sin\alpha \end{Bmatrix}\right]\left[1+\sqrt{\varepsilon}\sin(\theta+\alpha)+\varepsilon\right]^{\frac{1}{2}}.$$

To find the fields $\vec{E}^a_\omega$ and $\vec{H}^a_\omega$, we use solution of the corresponding "etalon" problem (determining EM field in the bulk of the target). Omitting cumbersome calculations, we

* Supported by Russian Science Foundation (Grant No. 18-72-10137).
† s.galyamin@spbu.ru

ISBN: 978-3-95450-208-0 doi:10.18429/JACoW-IPAC2019-MOPGW060

get for azimuthal field components for $\rho|s| \gg 1$ at the inner side of the outer surface [13]:

$$H^{a-}_{\varphi\omega} = \frac{q\omega \exp\left(ik_0 z_0/\beta + i\rho_0 s - 3\pi i/4\right)}{i\pi v^2\gamma^2}\sqrt{\frac{2}{\pi\rho_0 s}}\times$$
$$\times\frac{ik_0}{s^2}\Bigg\{-\varepsilon s I_0(r_0\sigma_0)\tilde{A}^{(E2)}_0 + 2\sum_{\nu=1}^{\infty} I_\nu(r_0\sigma_0)e^{\frac{i\pi(1-\nu)}{2}}\times \qquad (3)$$
$$\times\cos(\nu\varphi)\left[\varepsilon\tilde{A}^{(E2)}_\nu\left(is-\frac{1}{2\rho_0}\right)-\frac{i\nu}{\beta\rho_0}\tilde{A}^{(H2)}_\nu\right]\Bigg\},$$

$$E^{a-}_{\varphi\omega} = \frac{q\omega \exp\left(ik_0 z_0/\beta + i\rho_0 s - 3\pi i/4\right)}{i\pi v^2\gamma^2}\sqrt{\frac{2}{\pi\rho_0 s}}\times$$
$$\times\frac{ik_0}{s^2}2\sum_{\nu=1}^{\infty} I_\nu(r_0\sigma_0)e^{\frac{i\pi(1-\nu)}{2}}\times \qquad (4)$$
$$\times\sin(\nu\varphi)\left[i\tilde{A}^{(H2)}_\nu\left(is-\frac{1}{2\rho_0}\right)-\frac{\nu}{\beta\rho_0}\tilde{A}^{(E2)}_\nu\right],$$

where $s^2 = k_0^2\beta^{-2}(\varepsilon\beta^2-1)$, $s = \sqrt{s^2}$, $\mathrm{Im}\sqrt{\ } > 0$, $\sigma_0^2 = k_0^2\beta^{-2}(1-\beta^2)$, $\sigma_0 = \sqrt{\sigma_0^2}$, $\mathrm{Re}\sqrt{\ } > 0$, I_ν is a modified Bessel function, γ is a Lorentz factor, $\tilde{A}^{(E2)}_\nu$ and $\tilde{A}^{(H2)}_\nu$ are coefficients determined from linear system based on boundary conditions for $\rho = a$ (see [13] for details). Component $H_{\varphi\omega}$ determines "parallel" polarization ($\parallel$) containing components $E_{z\omega}$, $E_{\rho\omega}$ and $H_{\varphi\omega}$ with corresponding Fresnel coefficient

$$T_\parallel = 2\cos\theta_i\left(\cos\theta_i + \sqrt{\varepsilon}\cos\theta_t\right)^{-1}.$$

Component $E_{\varphi\omega}$ determines "orthogonal" polarization ($\perp$) containing components $H_{z\omega}$, $H_{\rho\omega}$ and $E_{\varphi\omega}$ with corresponding Fresnel coefficient

$$T_\perp = 2\sqrt{\varepsilon}\cos\theta_i\left(\sqrt{\varepsilon}\cos\theta_i + \cos\theta_t\right)^{-1}.$$

Angle of incidence θ_i can be obtained from Snell's law $\sqrt{\varepsilon}\sin\theta_i = \sin\theta_t$ and angle of refraction θ_t:

$$\sin\theta_t = \frac{-1}{\beta\sqrt{r^2+r'^2}}\Big[r\sin\theta - r'\cos\theta -$$
$$-\sqrt{\varepsilon\beta^2-1}\,(r\cos\theta + r'\sin\theta)\Big], \quad r' = dr/d\theta.$$

Unit vector of transmitted wave $\vec{e}_k$ is

$$e_{k\rho} = n_\rho\cos\theta_t - n_z\sin\theta_t, \quad e_{kz} = n_\rho\sin\theta_t + n_z\cos\theta_t.$$

Transmitted fields at the outer surface of the aperture are:

$$H^a_{\varphi\omega} = T_\parallel H^{a-}_{\varphi\omega}, \quad \vec{E}^\parallel_\omega = H^a_{\varphi\omega}\left[\vec{e}_\varphi, \vec{e}_k\right],$$
$$E^a_{\varphi\omega} = T_\perp E^{a-}_{\varphi\omega}, \quad \vec{H}^\perp_\omega = E^a_{\varphi\omega}\left[\vec{e}_k, \vec{e}_\varphi\right],$$
$$E^a_{\rho\omega} = H^a_{\varphi\omega}e_{kz}, \quad E^a_{z\omega} = -H^a_{\varphi\omega}e_{k\rho},$$
$$H^a_{\rho\omega} = -E^a_{\varphi\omega}e_{kz}, \quad H^a_{z\omega} = E^a_{\varphi\omega}e_{k\rho}.$$

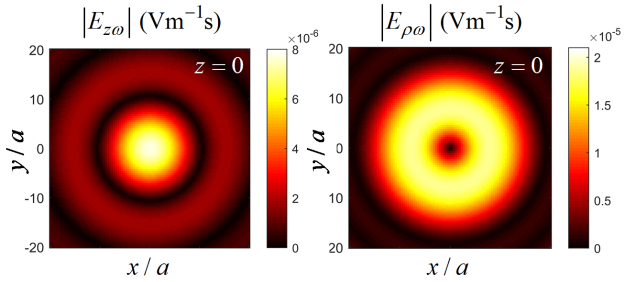

Figure 2: Two dimensional distribution of absolute values of $E_{z\omega}$ and $E_{\rho\omega}$ over xy-plane for symmetrical case $r_0 = 0$. in the focal plane.

NUMERICAL RESULTS

For evaluation of integrals (2), a numerical code was realized in MATLAB with the use of Parallel Computing Toolbox. Parameters for calculations are: $\omega = 2\pi\cdot 100\,\mathrm{GHz}$, $\beta = 0.8$, $f = 500c/\omega$, $z_f = 0$, $q = 1\mathrm{nC}$, $\varphi_0 = 0$, $x_{\max} = 500c/\omega$, $x^{\mathrm{eff}}_{\max} = 340c/\omega$, $a = c/\omega$, $\theta_{\min} = 162°$, $\theta_{\max} = 179°$, $\varepsilon = 1.6$, $\alpha = 80°$, $\alpha_{\mathrm{tar}} = 73°$. We will restrict ourselves by taking into account only three modes in Eqs. (3) and (4) which is enough up to $r_0 = a/2$.

Figure 2 shows two-dimensional distribution of longitudinal ($E_{z\omega}$) and transverse ($E_{\rho\omega}$) components over xy-plane for $z = 0$ and symmetric case $r_0 = 0$. As one can clearly see, transverse field is exact zero on the symmetry axis while longitudinal field is maximal here. Transverse field quickly increases with observation point shift from z-axis and has its maximum value around two times larger compared to maximum of $E_{z\omega}$. Total field is practically determined by transverse field excluding small central area.

The case with a shifted charge is shown in Fig. 3. Magnitudes of transverse and longitudinal fields differ approximately by factor 5 and increase almost linearly with increasing r_0. The most interesting feature is occurred in longitudinal field. For relatively small offset ($r_0 = a/10$), this field is strongly asymmetric with respect to $x = 0$. The stronger peak is located in the area $x > 0$, i.e. in the area where shifted charge propagates (recall that a charge is shifted to positive x). With an increase in r_0 these peaks become more symmetrical ($r_0 = a/4$), and for relatively large offset ($r_0 = a/2$) we have two almost symmetrical peaks located approximately at $x = 6.7a$ and $x = -8.7a$, i.e. far enough from the charge trajectory. More detailed position of the discussed peaks is shown in Fig. 4. In turn, transverse field also has an essential asymmetry for relatively small offset. It is worth noting that the peak of transverse field is shifted in opposite direction compared to the shift of the charge trajectory, its approximate location is $x = -2.3a$ (see Fig. 4 for details). For larger offsets, the peak of $E_{\rho\omega}$ becomes practically symmetric in both x and y direction, is located nearly in the center and dominates the longitudinal peak.

Possible applications of the presented dielectric concentrator would lie in the area of beam diagnostics and beam manipulation. Since strong field concentration takes place

ISBN: 978-3-95450-208-0 doi:10.18429/JACoW-IPAC2019-MOPGW060

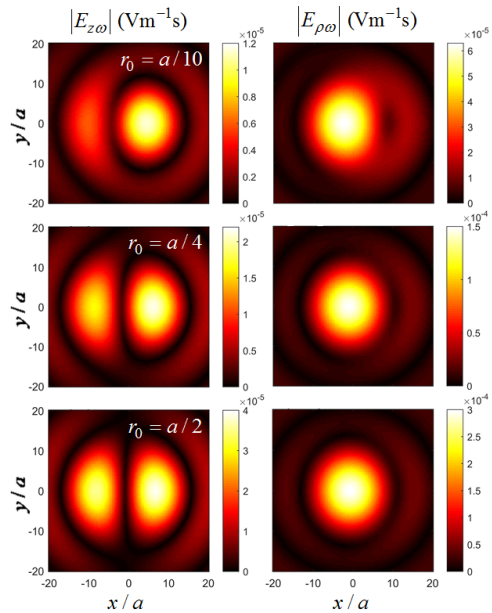

Figure 3: Two dimensional distribution of absolute values of $E_{z\omega}$ and $E_{\rho\omega}$ over xy-plane in the focal plane for $r_0 = a/10$, $a/4$, $a/2$.

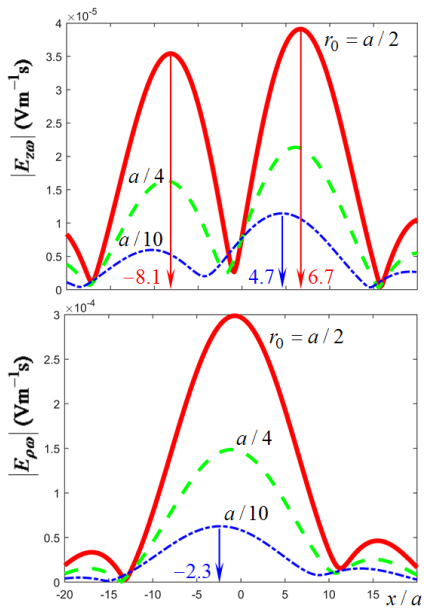

Figure 4: Dependence of absolute values $E_{z\omega}$ and $E_{\rho\omega}$ on x for $y = z = 0$ and $r_0 = a/10$, $a/4$, $a/2$.

in the focal plane near the focal point, sensitivity and accuracy of mentioned diagnostics can be essentially increased. For example, peculiarities of field distribution for $r_0 \neq 0$ can be used for determination of beam shift and positioning the beam to the axis of the structure. Note that difference between magnitudes of two peaks of top plot in Fig. 4 depends on r_0. For $r_0 = a/10$, left peak magnitude is about 50% of the right peak magnitude while for $r_0 = a/2$ left peak magnitude is about 90% of the right peak magnitude. Moreover, these peaks are shifted for several values of a (in our case from ≈ 5 to ≈ 8) from the axis thus simplifying the detection of the field.

If the bunch is well aligned along the axis ($r_0 = 0$), it experiences influence of longitudinal field ($E_{z\omega}$) only, see Fig. 2. Interaction between the bunch and strongly concentrated radiated field can lead to longitudinal modulation of the bunch. If the bunch is shifted ($r_0 \neq 0$), it is affected by strong transverse field in the focal plane. Therefore, the concentrator can operate as all-dielectric transverse kicker in this case.

REFERENCES

[1] C. Jing, S. Antipov, M. Conde, W. Gai, G. Ha, W. Liu, N. Neveu, J. Power, J. Qiu, J. Shi, D. Wang, and E. Wisniewski, *Nucl. Instrum. Meth. Phys. Res. A*, vol. 898, p. 72, 2018.

[2] B.D. O'Shea, G. Andonian, S. Barber, K. Fitzmorris, S. Hakimi, J. Harrison, P.D. Hoang, M.J. Hogan, B. Naranjo, O.B. Williams, V. Yakimenko, and J. Rosenzweig, *Nat. Communications*, vol. 7, p. 12763, 2016.

[3] D. Wang, X. Su, L. Yan, Y. Du, Q. Tian, Y. Liang, L. Niu, W. Huang, W. Gai, C. Tang, and S. Antipov, *Appl. Phys. Lett.*, vol. 111, p. 174102, 2017.

[4] N. Sei and T. Takahashi, *Scientific Rep.*, vol. 7, p. 17440. 2017.

[5] A.P. Potylitsyn, S.Y. Gogolev, D.V. Karlovets, G.A. Naumenko, Y.A. Popov, M.V. Shevelev, and L.G. Sukhikh, "Coherent Cherenkov Radiation from a Short bunch Passing near a Target and Possibility of a Bunch Length Diagnostics", in *Proc. IPAC'10*, Kyoto, Japan, May 2010, paper MOPE046, pp. 1074–1076.

[6] R. Kieffer, L. Bartnik, M. Bergamaschi, V.V. Bleko, M. Billing, L. Bobb, J. Conway, M. Forster, P. Karataev, A.S. Konkov, R.O. Jones, T. Lefevre, J.S. Markova, S. Mazzoni, Y. Padilla Fuentes, A.P. Potylitsyn, J. Shanks, and S. Wang, *Phys. Rev. Lett.*, vol. 121, p. 054802, 2018.

[7] S.N. Galyamin, A.V. Tyukhtin, and V.V. Vorobev, *J. Instrumentation*, vol. 13, C02029, 2018.

[8] A.V. Tyukhtin, S.N. Galyamin, and V.V. Vorobev, *Phys. Rev. A*, vol. 99, p. 023810, 2019.

[9] A.V. Tyukhtin, V.V. Vorobev, S.N. Galyamin, and E.S. Belonogaya, *Phys. Rev. Accel. Beams*, vol. 22, p. 012802. 2019.

[10] S.N. Galyamin and A.V. Tyukhtin, *Phys. Rev. Lett.*, vol. 113, p. 064802, 2014.

[11] S.N. Galyamin, A.V. Tyukhtin, and V.V. Vorobev, *Nucl. Instrum. Meth. Phys. Res. B*, vol. 402, p. 144, 2017.

[12] A.Z. Fradin, *Microwave Antennas* , Pergamon, 1961.

[13] S.N. Galyamin, V.V. Vorobev and A.V. Tyukhtin, `arXiv:1904.05188`, 2019.